

Article

Study on the Properties and Mechanism of Recycled Aggregate/Asphalt Interface Modified by Silane Coupling Agent

Jiawang Zhou ^{1,*}, Kui Hu ^{1,*}, Junfeng Gao ^{2,*}, Yujing Chen ¹, Qilin Yang ³ and Xiaotong Du ¹

¹ College of Civil Engineering and Architecture, Henan University of Technology, Zhengzhou 450001, China; zjw0172@163.com (J.Z.); yujingchen@haut.edu.cn (Y.C.); duxiaotong0601@163.com (X.D.)

² College of Materials Science and Engineering, Chongqing Jiaotong University, Chongqing 400074, China

³ School of Transportation Science and Engineering, Harbin Institute of Technology, Harbin 150090, China; qilin.yang@hit.edu.cn

* Correspondence: mailhukui@haut.edu.cn (K.H.); jfgao@cqjtu.edu.cn (J.G.)

Abstract: The use of recycled concrete aggregates (RCA) instead of natural aggregates in hot-mix asphalt mixtures is one of the ways to achieve energy savings and reduce carbon emissions in road engineering. However, the cement mortar on the surface of RCA adversely affects the adhesion properties between asphalt and aggregates, leading to a reduction in the performance characteristics of asphalt mixtures. In this study, a silane coupling agent (SCA) was employed to improve the adhesion properties of the RCA/asphalt interface. The enhancement mechanism of SCA on the RCA/asphalt interface was investigated from multiple perspectives, including macroscopic properties, interfacial microstructure, and nanoscale interfacial interactions. Firstly, the adhesion behavior and tensile strength of the interface between RCA and asphalt were determined through a boiling water test and direct tensile test, both before and after SCA modification. Secondly, scanning electron microscopy (SEM) was employed to observe the surface microstructure of RCA and the microstructure of the RCA/asphalt interface. Finally, the main component of mortar, calcium silicate hydrate (C-S-H), was taken as the research subject of investigation to examine the hydrogen bonding, interaction energy, and interface transition zone of the C-S-H/asphalt interface system using the molecular dynamics methodology. The results demonstrate a two-level enhancement in the adhesion performance of the interface at the macroscopic scale following SCA modification. The interface tensile strength increased by 72.2% and 119.7% under dry and wet conditions, respectively. At the microscopic scale, it was observed that the surface pores of RCA were repaired after SCA modification, resulting in a more tightly bonded interface between the RCA and asphalt. At the nanoscale, SCA modification reduces the hydrophilicity of the C-S-H surface, increases the interaction energy and water resistance of the C-S-H/asphalt interface, and enhances the weak interface transition zone between C-S-H and asphalt. This study provides a theoretical basis for using SCA to enhance the bond strength of the RCA/asphalt interface and lays the foundation for the application of RCA asphalt mixtures on highways.

Keywords: silane coupling agent; recycled concrete aggregates; RCA/asphalt interface; interface reinforcement mechanism; molecular dynamic



Citation: Zhou, J.; Hu, K.; Gao, J.; Chen, Y.; Yang, Q.; Du, X. Study on the Properties and Mechanism of Recycled Aggregate/Asphalt Interface Modified by Silane Coupling Agent. *Appl. Sci.* **2023**, *13*, 10343. <https://doi.org/10.3390/app131810343>

Academic Editor: Luís Picado Santos

Received: 7 August 2023

Revised: 8 September 2023

Accepted: 13 September 2023

Published: 15 September 2023



Copyright: © 2023 by the authors. Licensee MDPI, Basel, Switzerland. This article is an open access article distributed under the terms and conditions of the Creative Commons Attribution (CC BY) license (<https://creativecommons.org/licenses/by/4.0/>).

1. Introduction

The amount of construction trash produced each year has increased significantly as a result of the fast urbanization and infrastructural development. However, the utilization rate of solid waste during construction is still very low [1–4]. On the other hand, mining natural aggregates can lead to irreversible ecological damage in mountainous areas, while the processing and transportation processes result in high carbon emissions, highlighting the increasingly prominent environmental and social issues [5–7]. In the context of global efforts to promote energy conservation and emission reduction, the transformation of

resource utilization in the construction industry, which involves replacing natural sand and stone with construction solid waste, emerges as the path for the industry to achieve carbon reduction goals and upgrade development [8–10]. With the continuous improvement of construction solid waste particle-size crushing and component-sorting technology, a large amount of uniformly shaped, clean, and high-purity recycled concrete aggregate (RCA) can be obtained, and the cost of using RCA is lower than that of natural aggregates [11–14]. Therefore, the application of RCA in asphalt pavement has significant environmental value and economic benefits [15].

The primary distinction between RCA and natural aggregates is that the surface absorbs a lot of cement mortar [16,17]. According to studies, the main factor that contributes to the inadequate adhesion of asphalt and aggregates is the existence of cement mortar on the surface of RCA [18,19]. The calcium silicate hydrate (C-S-H) in the cement mortar accounts for approximately 60–70% of the hydration products, and it is the principal component and strength source of cement hydration products [20]. However, the chemical bonding between C-S-H and asphalt is weak, which can easily lead to inadequate bond strength between the mortar and asphalt. On the other hand, the mortar pores and microcracks on the surface of RCA are plentiful, and water adsorbed by capillary action is difficult to discharge under natural conditions. Because asphalt is hydrophobic, the existence of water might cause damage to the RCA/asphalt interface [21]. Therefore, in order to add the amount of RCA blending and improve the performance of hot-mix asphalt mixtures, it is necessary to address the problem of inadequate chemical bonding between RCA and asphalt, as well as water damage to the interface.

For enhancing the basic properties of materials, many scholars have chosen different modification methods [22–26]. The addition of anti-spalling chemicals into asphalt mixtures is an efficient technique to boost binding strength and improve resistance to water damage at the asphalt/aggregate interface [27–29]. At the moment, the most popular anti-spalling agent is silane coupling agent (SCA), which is widely applied to enhance the interface binding strength of organic and inorganic materials [30]. This is due mainly to the fact that its organic functional groups and hydrolyzed groups can be chemically linked with organic and inorganic materials, respectively, which helps to improve the interfacial binding strength of organic and inorganic interface materials [31]. Due to the unique nature of SCA, its application in asphalt mixtures has attracted extensive attention from researchers. Li et al. [32] investigated the effect of SCA (KH550) on the adhesion properties between acidic aggregates and asphalt. They found that SCA can act as a molecular bridge to enhance the bond strength between asphalt and acidic aggregates. Ye et al. [33] conducted an analysis on the water stability of SCA-modified asphalt with aggregates, comparing it to SBS-modified asphalt and rock-modified asphalt. The study revealed that SCA-modified asphalt exhibited superior water stability when combined with aggregates. Ran et al. [34] modified oil sludge pyrolysis residue with SCA and found that the surface of the oil sludge pyrolysis residue became rough after treatment with KH550, forming strong physical and chemical adsorption between the oil sludge pyrolysis residue and asphalt.

Currently, most research on the interface between RCA/asphalt is conducted at a macroscopic level. However, the interaction between RCA and asphalt is a complex process that is easily influenced by interactions between different molecular groups. With current experimental techniques, it is still very difficult to understand the impact of SCA modification on the interaction for the RCA/asphalt interface [35]. It is now possible to know how SCA modification affects the interaction between RCA and the asphalt interface, as molecular dynamics simulation techniques have been widely used to investigate the interaction between asphalt and aggregates. Previous studies have used molecular dynamics simulations to establish molecular models of asphalt, aggregates, and C-S-H and have studied their interactions [36,37]. Sun et al. [38] explored the impact of interface water on the structure of asphalt and the interaction energy of the asphalt/aggregate interface and discovered that the existence of interface water altered the nanostructure of the asphalt and diminished the interaction energy of the interface.

Luo et al. [39] revealed that the anisotropy of aggregate surfaces significantly affects the interaction energy with asphalt and the water stability of the interface. Zhai et al. [40] investigated the effect of asphalt aging on the damage behavior of the asphalt/aggregate interface and found that asphalt aging reduced the thermodynamic properties of asphalt, such as surface free energy and cohesive energy. However, it also enhanced the adhesion strength between the asphalt/aggregate interface.

The above study primarily describes the influence of SCA modification on the interfacial performances through experimental methods. It also investigates the interaction relationship between the asphalt and aggregate using molecular dynamics. However, the influence of SCA modification on the interfacial performances and interaction relationship between RCA and asphalt has not yet been resolved. Therefore, the objective of this study is to explore the multi-scale enhancement mechanism of SCA modification on the interface between RCA and asphalt. First, at the macro-scale, the adhesion behavior and tensile strength of the interface between RCA and asphalt were determined before and after SCA modification using a boiling water test and direct tensile test. Second, on a micro-scale, the impact of SCA modification on the microstructure of the RCA/asphalt interface was observed through scanning electron microscopy. Finally, at the nanoscale, the main component of mortar, C-S-H, was taken as the research object to analyze the hydrogen bonding, interaction energy, and interface transition zone of the C-S-H/asphalt interface system using the molecular dynamics method.

2. Materials and Methods

2.1. Main Materials

This study utilized samples of RCA1 and RCA2 in different experimental tests. RCA1 is a cubic sample measuring $30 \times 30 \times 30$ mm, cut from a discarded cement column. It is used to measure the interfacial bond strength in direct tensile tests. RCA2 is obtained by crushing and sieving discarded concrete blocks to obtain samples with dimensions of 13.2–19 mm. It is used in boiling water tests to determine the adhesion properties for the RCA/asphalt interface. The RCA1 and RCA2 samples in this experiment needed to be cleaned and dried before the experiment to avoid the impact of surface pollutants on the experimental results. In addition, SCA (KH-550)-modified RCA was selected to enhance the interface properties. The physical parameters of KH-550 are shown in Table 1. The No. 70 base asphalt was chosen to evaluate the interfacial behavior between RCA and asphalt. The physical parameters of the base asphalt are presented in Table 2. All abbreviations in this paper are shown in Table 3.

Table 1. Physical parameters of KH-550 coupling agent.

Physical Parameters	Units	Value	Test Standard
Boiling point	°C	73.6	ASTM D1078-11 [41]
Density	g/cm ³	48.0	ASTM D4052 [42]
Refractive index ND25	—	102.2	ASTM D542-14 [43]

Table 2. Physical parameters of No. 70 asphalt binder.

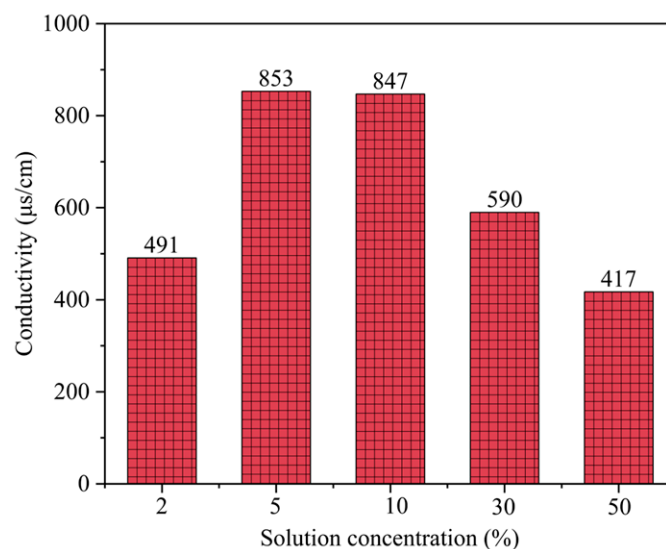
Physical Parameters	Units	Value	Test Standard
Penetration (25 °C, 100 g, 5 s)	0.1 mm	73.6	ASTM D5-06 [44]
Softening point	°C	48.0	ASTM D36-06 [45]
Ductility (15 °C, 5 cm/min)	cm	102.2	ASTM D113-07 [46]

Table 3. All prefixes in this paper.

Prefix	Full Name
RCA	Recycled concrete aggregate
RCA1	Discarded cement column (30 × 30 × 30 mm)
RCA2	Recycled concrete aggregate (13.2–19 mm)
C-S-H	Calcium silicate hydrate
SCA	Silane coupling agent
SEM	Scanning electron microscopy
SARA	Saturates, aromatics, resins, and asphaltenes

2.2. Treatment Methods and Reaction Mechanisms

In this study, deionized water and ethanol were chosen as solvents for the hydrolysis reaction of SCA. In addition, to determine the optimal concentration of SCA, conductivity was chosen as a measure to assess the effect of concentration on the degree of SCA hydrolysis. This is because the conductivity of SCA and deionized water is very low, while the conductivity of the hydrolysis products of SCA is high. In addition, in the solution proportioning, there is no effect on the conductivity of the system because ethanol always makes up 50% of the total solution volume in the solution proportion. Therefore, the degree of hydrolysis of the SCA can be confirmed through conductivity measurements. As shown in Figure 1, the conductivity increased significantly when the SCA concentration was increased from 2% to 5%. However, as the SCA concentration continued to increase, the conductivity did not increase; instead, it showed a decreasing trend. The results indicate that the hydrolysis of SCA is highest when the concentration of SCA is 5%. Therefore, the optimal ratio of the SCA mixture solution is SCA:deionized water:ethanol = 5:45:50.

**Figure 1.** Conductivity of SCA mixed solutions at various concentrations.

The RCA treatment method and modification mechanism are shown in Figure 2. First, the SCA mixed solution (SCA:distilled:ethanol = 5:45:50) was stirred at 60 °C for 30 min to promote the hydrolysis reaction of SCA. Then, the RCA was immersed in an SCA mixture for 30 min to ensure a sufficient reaction between the SCA and RCA. Finally, the RCA was dried at a high temperature of 160 °C for 60 min to undergo a dehydration condensation reaction. During the entire process, the methoxy group (–OCH₃) in the molecular structure of SCA (KH550) can hydrolyze into the alkoxy group (–SiOH) of silanol in a mix of ethanol and water. Then, under high temperature conditions, the alkoxy group undergoes a dehydration condensation reaction with the hydroxyl group on the RCA surface to form Si–O–Si bonds [47].

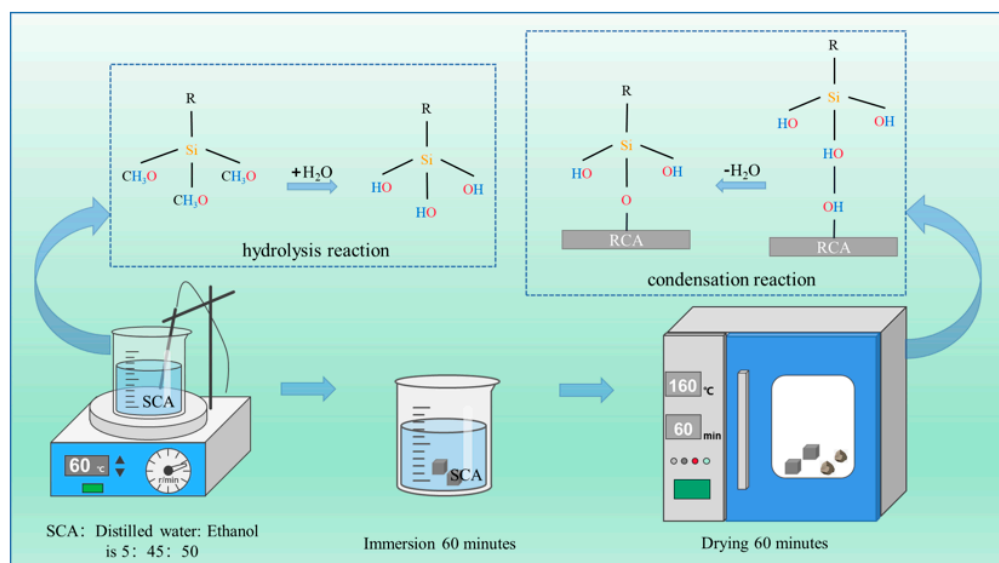


Figure 2. RCA treatment method and modification mechanism.

2.3. Experimental Testing Methods

2.3.1. Boiling Water Test

The boiling water test is a commonly used method to test the adhesion performance of asphalt to aggregate surfaces and evaluate the aggregate’s resistance to water stripping. According to ASTM D36-25 [48] and the Chinese boiling test, the specific steps of the experiment are as follows. First, tie the RCA with wire and place it in a 105 °C drying oven to dry. Then, immerse the dried RCA in asphalt at 140 °C for 45 s, remove it, and cool it at room temperature for 15 min. Finally, immerse it in boiling water for 3 min, remove it, and observe the degree of asphalt film peeling on the surface of the RCA to evaluate its adhesion grade according to Table 4.

Table 4. Grade of adhesion of RCA to asphalt.

The Degree of Asphalt Film Spalling on the Surface of RCA after Boiling Water Test	Adhesion Grade
The asphalt film is not damaged and there is no peeling.	5
The thickness of the RCA surface asphalt film is uneven, with a peeling area percentage of less than 10%.	4
The asphalt film is generally retained on the surface of the RCA, with a peeling area percentage of less than 10%.	3
The asphalt film is partially retained on the surface of the RCA, with a peeling area percentage greater than 30%.	2
The surface asphalt film of the RCA has mostly peeled off, allowing the asphalt to float on the water’s surface.	1

2.3.2. Direct Tensile Test

The direct tensile test is a crucial method for determining the interface characteristic parameters of asphalt mixtures. This test can be used to assess the fracture performance of the asphalt mixtures. In this study, the direct tensile test was used to examine the influence of SCA modification on the bonding strength of the interface in RCA asphalt mixtures. To prepare the samples, RCA and asphalt were placed in an oven at 170 °C for approximately 30 min. Then, 1.2 g of melted asphalt was dropped onto the RCA surface and evenly spread. Another RCA was then pressed on top. Considering that water penetration into the RCA/asphalt interface may cause damage, the samples were divided into two groups. The first group was tested directly, while the second group was submerged in water for 24 h before testing. Before the experiment, the RCA was secured to the tensile device using epoxy resin adhesive. The loading rate of the tensile test equipment (CTM6001) was

set at 0.5 mm/min. The adhesion rate of asphalt on the RCA surface was determined by conducting a black and white image binarization analysis on the side of the RCA surface with less asphalt adhesion after stretching. Three sets of experiments were conducted for each experimental condition, and the average value of the three sets of experiments was calculated. If the ratio of the average value to the maximum or minimum value exceeds 10%, the investigation should be repeated.

2.3.3. SEM

This study utilizes SEM (Hitachi-S3400N) to observe the surface microstructure of RCA and the interface microstructure of RCA/asphalt. For the surface microstructure of RCA, RCA2 samples can be directly observed. For the RCA/asphalt interface microstructure, the intact RCA/asphalt interface was selected for observation after crushing the RCA1 samples. Then, the powder impurities generated at the interface were cleaned with anhydrous ethanol and observed after drying at room temperature (18–25 °C).

3. Simulation Methods

3.1. Computational Models

3.1.1. Asphalt Model

Asphalt is a residual petroleum mixture composed of hydrocarbons, sulfur and nitrogen compounds, and their non-metallic derivatives. These molecules have significant differences in polarity and molecular weight, making it difficult to represent their composition with a single molecule. In order to understand the molecular structure of asphalt, Jennings et al. constructed an average molecular structure based on the nuclear magnetic resonance (NMR) spectra of eight asphalt samples from the Strategic Highway Research Program (SHRP) in the United States. However, these structures cannot reflect the interactions between asphalt components. Subsequently, the asphalt system was divided into four components: saturates, aromatics, resins, and asphaltenes (SARA) using the standard test method (ASTM D4124-09 [49]). Through continuous improvement, Li and Greenfield constructed three 12-component asphalt models (AAA-1, AAK-1, and AAM-1) based on the SARA components. Therefore, in this study, the AAA-1 asphalt 12-component model was selected as a representative of the matrix asphalt for research. Figure 3 shows the molecular structure of the 12-component asphalt model. Figure 4 shows the model parameters of the 12-component asphalt model.

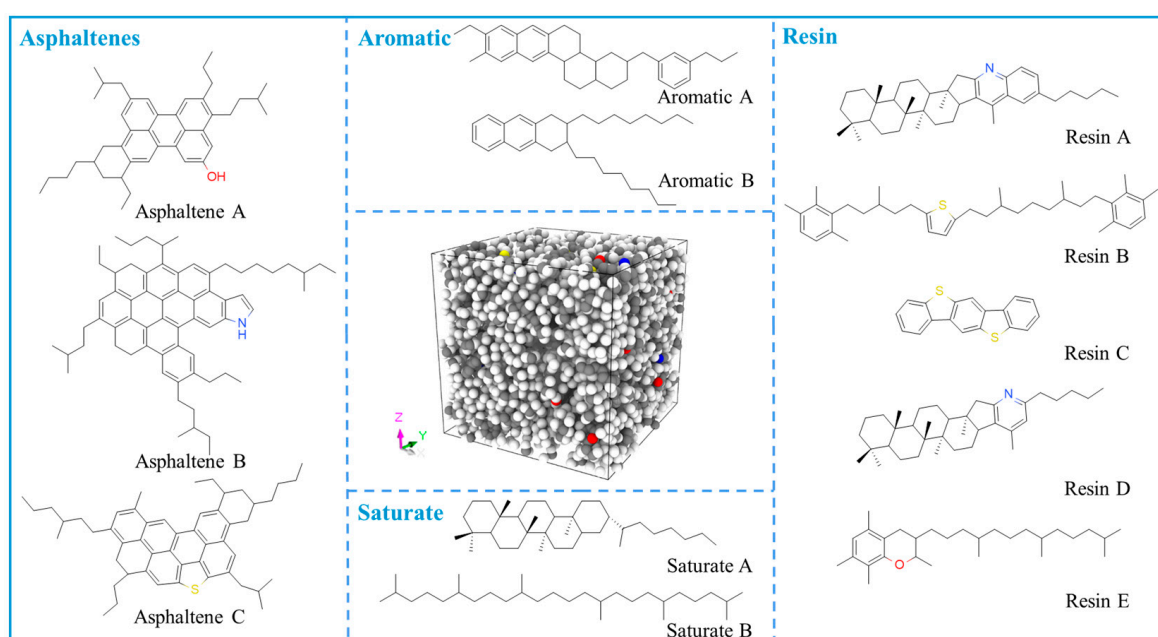


Figure 3. Asphalt 12-component model.

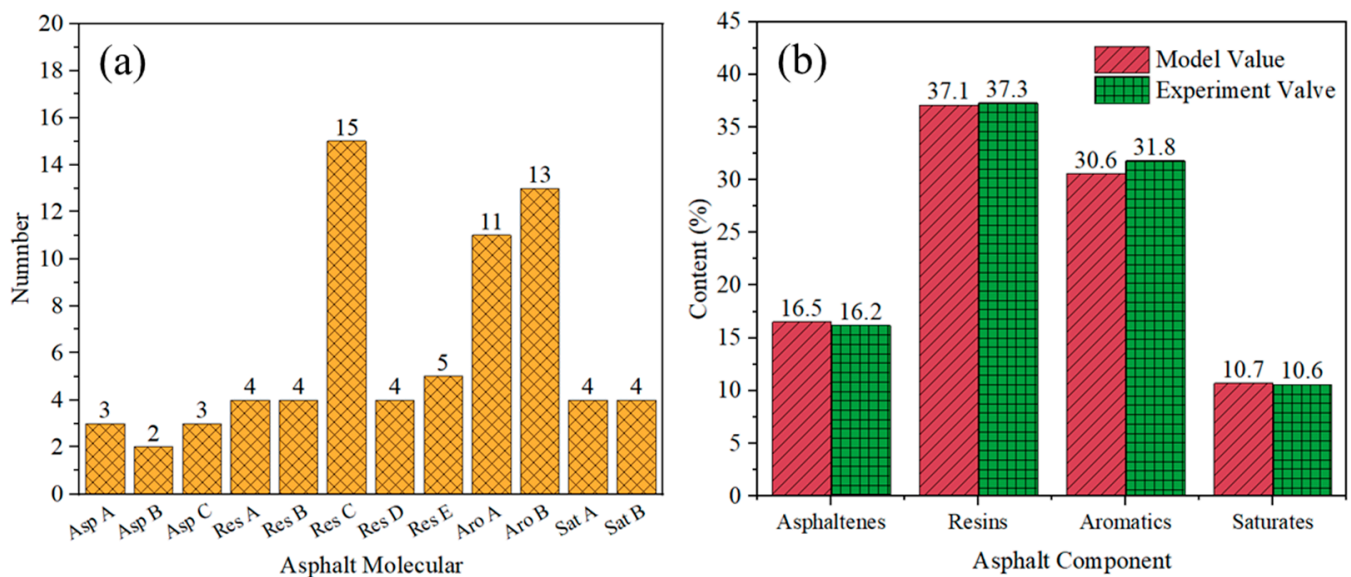


Figure 4. Asphalt 12-component model parameters: (a) the number of molecules; (b) the mass fraction of asphalt component.

In this study, the density and glass transition temperature (T_g) of the asphalt model were computed to verify the accuracy of the model. In this case, the density of asphalt was calculated using the isobaric–isothermal ensemble (NPT) at 1 atm pressure. As shown in Figure 5a, when the simulation time is greater than 30 ps, the density curve of the asphalt model tends to stabilize, so we calculated the average density of the asphalt model from 50 to 100 ps. From the analysis of the asphalt density curve, it can be concluded that the density of asphalt after equilibrium at 298 K is 1.02 g/cm^3 . The experimental density value of SHRP AAA-1 asphalt is $1.01\text{--}1.04 \text{ g/cm}^3$, which is consistent with the density of the asphalt model.

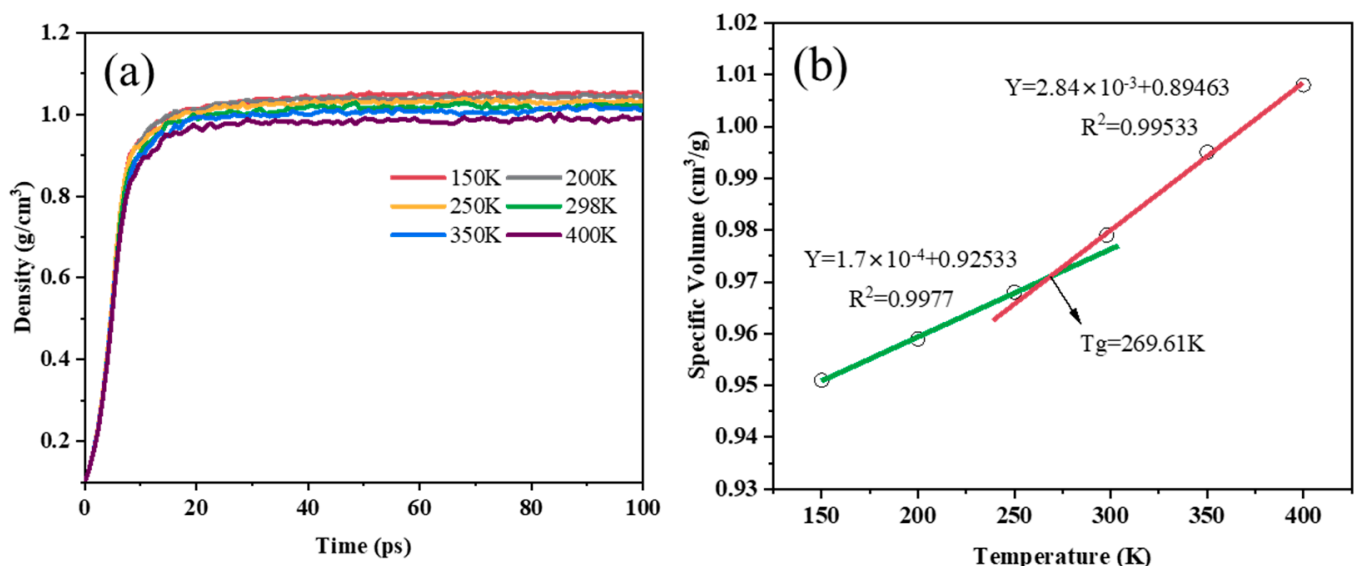


Figure 5. Physical properties of asphalt model: (a) density of asphalt; (b) glass transition temperature of asphalt.

After obtaining the asphalt density at different temperatures, the curve of asphalt specific volume (reciprocal of density) versus temperature was plotted, and linear regression analysis was performed. As shown in Figure 5b, the T_g of the asphalt is the intersection point of the two fitted lines. The T_g of the asphalt is lower than 273.15 K ($0 \text{ }^\circ\text{C}$), being at

269.61 K, which is consistent with previous research results [50–52]. Therefore, it can be considered that the asphalt model is reasonable.

3.1.2. SCA/C-S-H Model

For cement mortar adhered to RCA surfaces, C-S-H accounts for about 60–70% of the hydration products and is the main component and strength source of the hydration products [53,54]. In this study, a C-S-H model was established based on the method proposed by Pellenq et al., as shown in Figure 6. The specific steps are as follows: (1) Tobermorite 11 was used as the initial model. After removing the water molecules of the initial model, a $4 \times 3 \times 1$ supercell simulation was performed, and the monoclinic structure was changed to an orthorhombic one (Figure 6a); (2) To get the silicate chains to satisfy $Q1 = 11.63\%$, $Q2 = 67.44\%$, $Q3 = 20.93\%$, and $Ca/Si = 1.67$, some SiO_2 groups and Si_2O_5 groups were randomly removed from the silicate chains (Figure 6b); (3) The adsorption of water molecules to saturation was achieved using the grand canonical Monte Carlo (GCMC) method (Figure 6c); (4) To achieve equilibrium of model, the relaxation was continued under the NPT system (Figure 7d). Finally, the dimensions of the C-S-H model are $22.32 \text{ \AA} \times 22.17 \text{ \AA} \times 22.77 \text{ \AA}$. The density (2.45 g/cm^3) of the constructed model is close to the results obtained from previous simulations or experiments, indicating that the model is reasonably valid [55,56].

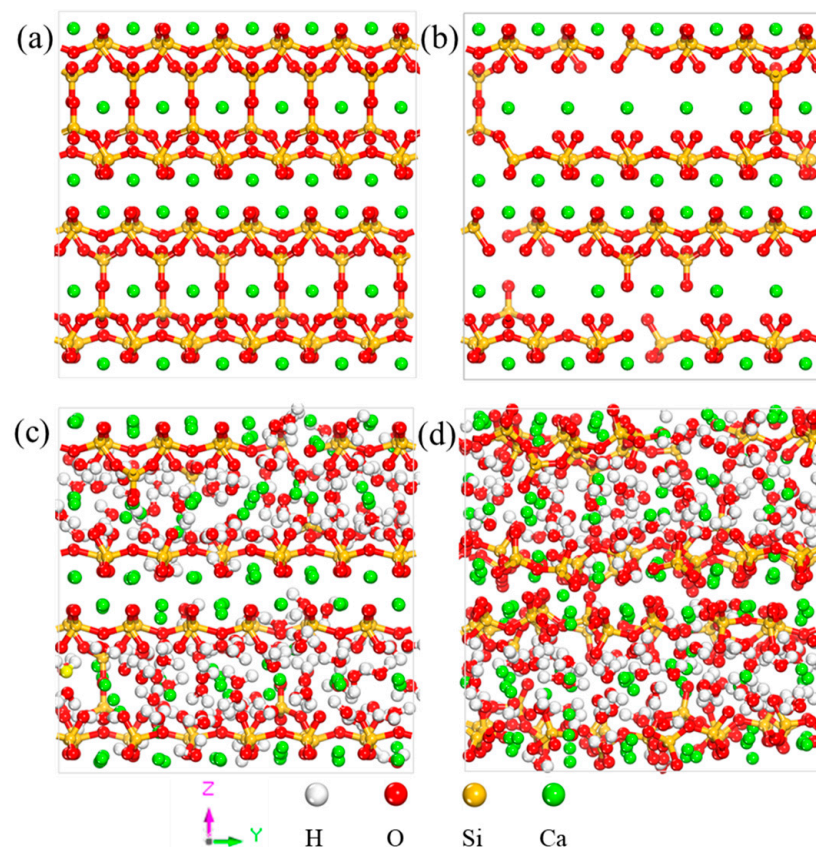


Figure 6. The construction of the C-S-H model (a) Orthogonal transformed model; (b) Remove some SiO_2 groups and dimer structures; (c) Absorb water molecules through the GCMC simulation; (d) Relax the model until equilibrium.

Figure 7 illustrates the establishment of the SCA/C-S-H model. Firstly, the C-S-H model $2 \times 2 \times 1$ supercell simulation was performed. Then, based on the SCA and cement mortar binding mechanism, the hydrolysis products of SCA were connected to the non-bridging oxygen atoms of the C-S-H matrix through Si-O-Si chemical bonding. The dimensions of the SCA/C-S-H model are $44.64 \text{ \AA} \times 44.34 \text{ \AA} \times 24.86 \text{ \AA}$.

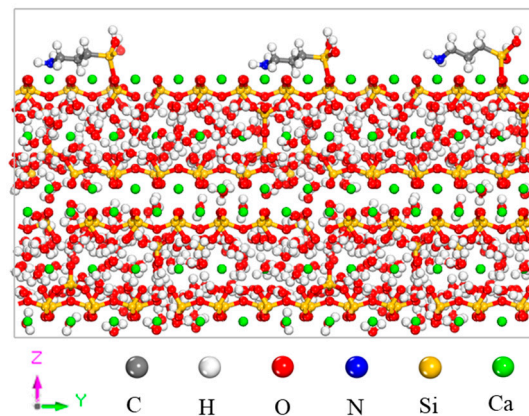


Figure 7. The SCA/C-S-H model.

3.1.3. C-S-H/Asphalt Interface Models

In this study, all simulations were performed using the Materials Studio 2020 software, and the COMPASS force field was selected to investigate the interaction mechanism of the C-S-H/asphalt interface. Taking the unmodified C-S-H model as an example, the asphalt/C-S-H interface model is shown in Figure 8a. For the placement of C-S-H and asphalt in the same simulation box, the dimensions of the C-S-H and asphalt models need to match in the x and y directions. Therefore, the asphalt model was first created with dimensions of $44.64 \text{ \AA} \times 44.34 \text{ \AA} \times 27.35 \text{ \AA}$ in the x, y, and z directions and subjected to 50,000 steps of geometry optimization. Next, the C-S-H model was expanded to a $2 \times 2 \times 1$ supercell with lattice parameters: $a = 44.64 \text{ \AA}$, $b = 44.34 \text{ \AA}$, and $c = 22.17 \text{ \AA}$. Then, the C-S-H/asphalt interface model was established, and a 30 \AA vacuum layer was added above the asphalt layer to eliminate periodic boundary effects. As shown in Figure 8b, based on the C-S-H/asphalt interface model, the influence of water on the interface bonding was studied by inserting a 2 \AA water layer between the C-S-H and asphalt layers. Finally, each interface model was relaxed for 500 ps under the canonical (NVT) ensemble, and the interface properties were analyzed using the trajectory from the last 100 ps.

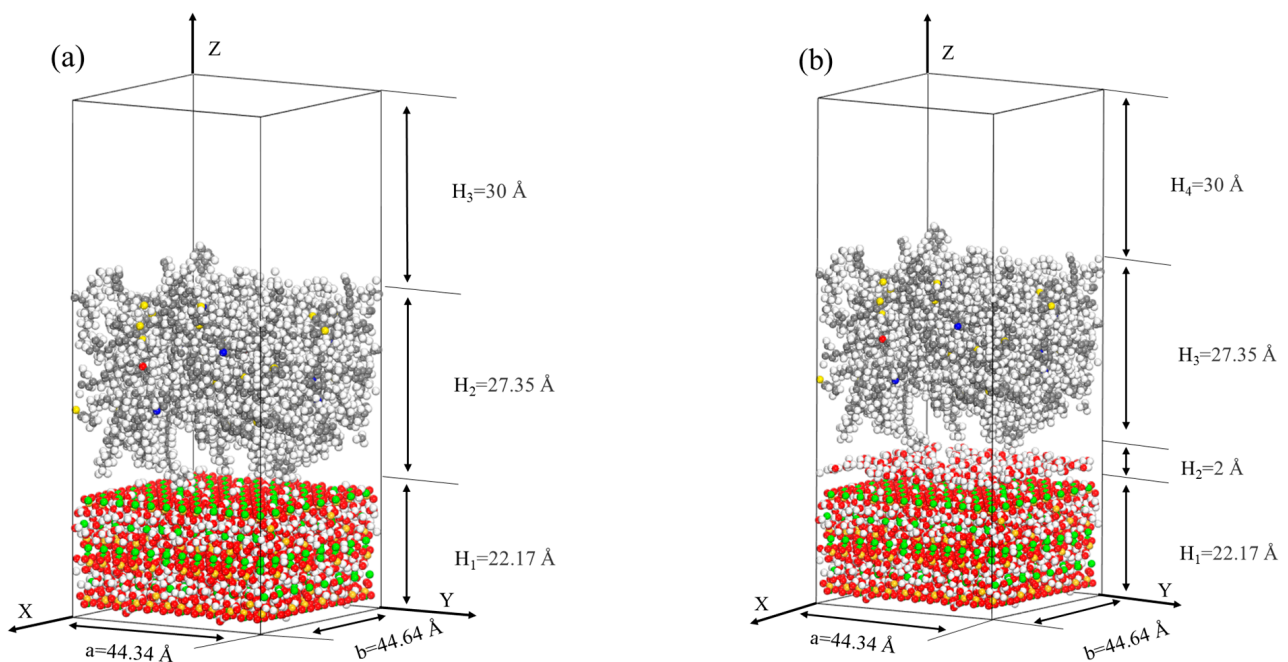


Figure 8. Interface models: (a) C-S-H/asphalt interface model; (b) C-S-H/water/asphalt interface model.

3.2. Simulation Calculations

3.2.1. Hydrogen Bond

Hydrogen bonding is a type of intermolecular interaction force formed between a hydrogen atom and an atom with a higher electronegativity, such as F, O, or N [57,58]. In this study, hydrogen bonding indirectly characterizes the interaction between the C-S-H surface and water molecules. The conditions for hydrogen bonding formation are as follows: (1) The distance between the hydrogen atom and the acceptor atom is less than 2.5 Å; (2) The donor-hydrogen-acceptor angle is less than 90°. The molecules providing the hydrogen atom and accepting the hydrogen atom are defined as the donor and acceptor, respectively.

3.2.2. Interaction Energy

The interaction energy can reflect the repulsive force and gravity of the C-S-H to the asphalt molecule [38,59]. From the molecular level, its main components include a covalent bond, van der Waals force, electrostatic electron, hydrogen bond, and so on. Here, the interaction energy can be calculated according to Equation (1).

$$E_{Asp-C-S-H} = E_{total} - (E_{Asp} + E_{C-S-H}) \quad (1)$$

where $E_{Asp-C-S-H}$ is the interaction energy between asphalt and C-S-H; E_{total} is the total potential energy of the entire interface system; E_{Asp} is the potential energy of asphalt; and E_{C-S-H} is the potential energy of C-S-H.

3.2.3. Relative Concentration

The interface transition zone refers to the region where different materials meet. In the C-S-H/asphalt system, the thickness of this zone is indicative of the extent to which asphalt is adsorbed onto the C-S-H surface. This research aims to determine the thickness of the interface transition zone by examining the relative concentration of asphalt and C-S-H in the Z direction. Furthermore, the study also investigates the impact of interface water on the nanostructure of asphalt by analyzing the relative concentration changes of the asphalt SARA components in the Z direction. At the same time, combined with the difference in the content of SARA components in the Z direction, the effect of interfacial moisture on the structure of the asphalt interface is discussed.

4. Results and Discussions

4.1. Boiling Water Test

The peeling condition of the asphalt film on the RCA surface before and after the boiling water test is shown in Figure 9. The results show that there is a significant difference in asphalt film stripping on the surface of RCA before and after SCA modification. Specifically, when the RCA is not modified by SCA, it can be observed that a large area of the asphalt film on the RCA surface peels off after the boiling water test, and the adhesion level is below grade 3 as shown in Table 4. This is because the surface of the aggregate absorbs a considerable amount of cement mortar, and there are massive pores on the surface. When a large number of pores exists on the surface of RCA, it will cause structural defects at the interface between the RCA and asphalt. During the boiling water experiment, the high temperature causes the gas inside the pores of the RCA to expand. This expansion leads to the destruction of the interface between the RCA and the asphalt, resulting in further shedding of the asphalt on the aggregate surface. This results in poor adhesion between asphalt and RCA and a weak interface transition zone. When RCA was modified by SCA, the asphalt film on the surface of RCA remained relatively intact after the boiling water experiment, and no apparent bubbles were observed in the boiling water experiment. According to Table 4, it can be concluded that the adhesion grade of the RCA asphalt mixture reached grade 5. This indicates that the SCA modification improves the interface properties of the RCA asphalt mixture.

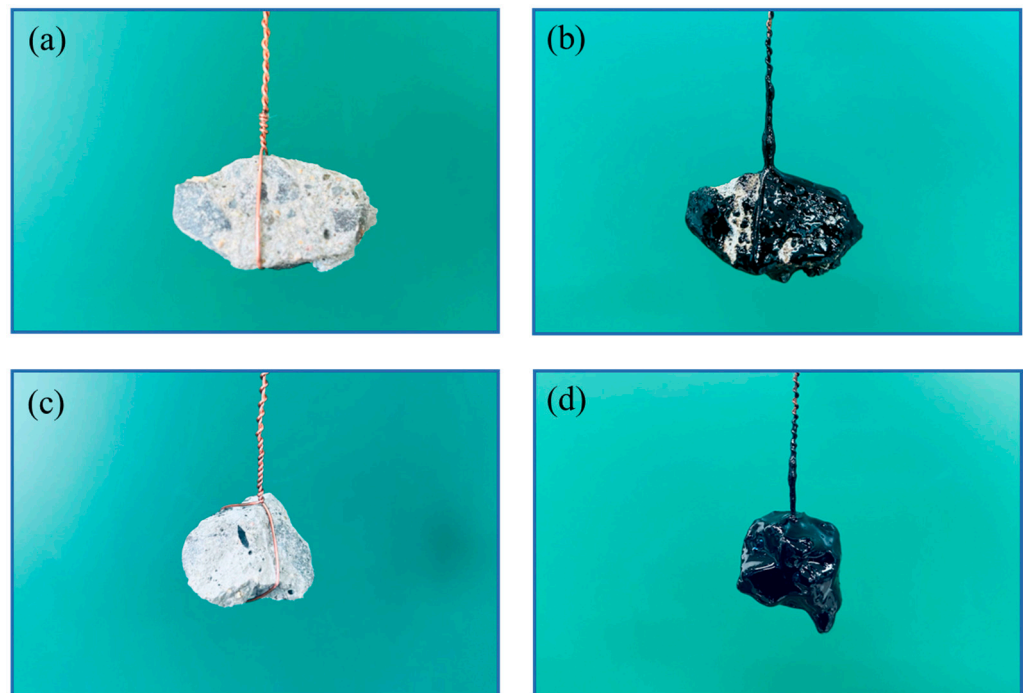


Figure 9. Boiling water test: (a) unmodified RCA before the test; (b) unmodified RCA after the test; (c) SCA-modified RCA before the test; (d) SCA-modified RCA after the test.

4.2. Direct Tensile Strength Test

The tensile strength of the interface between the RCA and asphalt is shown in Figure 10. The results indicate that the interface tensile strength significantly increases after SCA modification under both dry and wet conditions. Under dry conditions, the interface tensile strength between RCA and asphalt without SCA modification is 97 kPa. After SCA modification, the interface tensile strength increases by 72.2%. Under wet conditions, the interface tensile strength without SCA modification decreases by 56%. After SCA modification, the interface tensile strength increases by 119.7%.

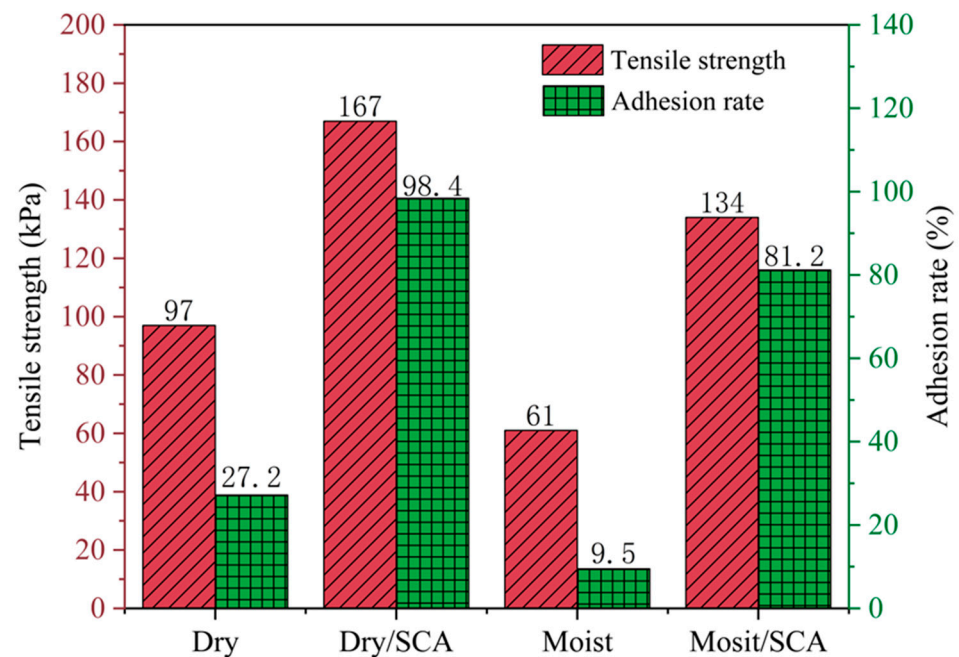


Figure 10. The tensile strength of the interface and adhesion rate of asphalt on RCA surface.

The influence of SCA modification on the interface failure types was analyzed by the interface failure forms shown in Figure 11 and the corresponding adhesion rates in Figure 10. The results showed that the adhesion rate of asphalt on the surface of RCA increased after SCA modification, changing the form of interface failure. In the unmodified RCA, the main type of interface failure was adhesion failure between the asphalt and RCA, with an adhesion rate of approximately 27.2%. However, after SCA modification, the type of interface failure was mostly cohesive failure, and the adhesion rate increased significantly to 98.4%. This is because when the adhesive force of the RCA/asphalt interface is greater than the cohesive force of asphalt itself, the asphalt undergoes cohesive failure. This indicates that SCA modification reinforces the adhesive strength of the interface, making the adhesive force more significant than the cohesive force of asphalt itself. At the same time, SCA modification also showed good performance under wet conditions, increasing the adhesion rate from 9.5% in the unmodified state to 81.2%.

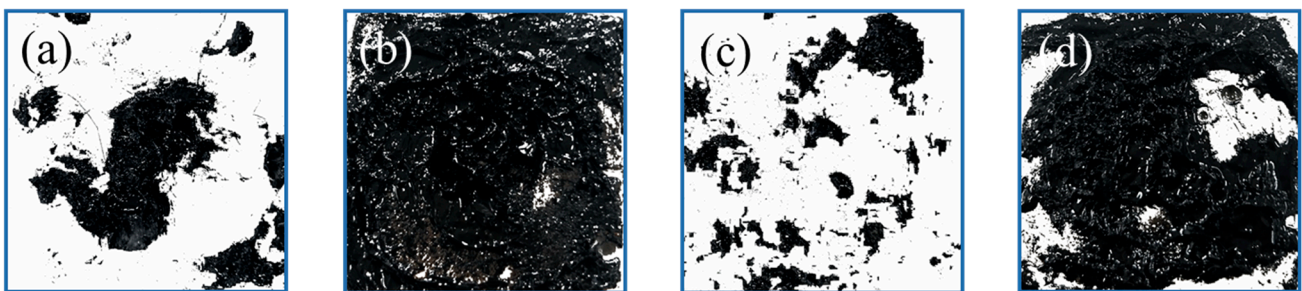


Figure 11. The fracture surface of RCA after binarization: (a) no modification under dry conditions; (b) SCA modification under dry conditions; (c) no modification under moist conditions; (d) SCA modification under moist conditions.

4.3. Microstructure Analysis

The surface microstructure of the RCA is shown in Figure 12. The results indicate that the surface porosity of the RCA is repaired after SCA modification, resulting in a tighter bond between the RCA and the interface. In terms of the surface microstructure of the RCA, without SCA modification, there are a large number of mortar pores on the RCA surface, which is the main reason for the high water absorption and poor adhesion performance of the RCA to asphalt. After SCA modification, the mortar pores of the RCA surface are significantly reduced. The reason for the reduction in surface pores of the RCA is that SCA first undergoes hydrolysis to form silanol, which then undergoes a condensation reaction with the hydroxyl groups on the cement mortar surface, resulting in the coverage of the cement mortar surface with alkyl-terminated siloxane, forming chemical adsorption.

The interface microstructure of the RCA/asphalt is shown in Figure 13. In terms of the interface structure between the RCA and asphalt, without SCA modification, the presence of a large number of pores on the RCA surface leads to defects in the RCA/asphalt interface structure. After SCA modification, the bond between the RCA and asphalt interface becomes denser. This is mainly because one end of the hydrolysis product of SCA is tightly adsorbed on the RCA surface, while the organic functional groups extend into the asphalt, tightly connecting the RCA and the asphalt. It acts as a “molecular bridge” between the RCA and asphalt interface, tightly connecting the RCA and asphalt together and improving the interface properties between the asphalt and RCA.

4.4. Hydrogen Bonding Analysis

In this study, we primarily calculated the number of hydrogen bonds formed between interfacial water and the C-S-H surface to investigate the effect of SCA alteration on the hydrophilicity of the C-S-H surface. As shown in Figure 14, the hydrogen bonds at the interface mainly form between water molecules and the silicate chains, as well as between water molecules and SCA.

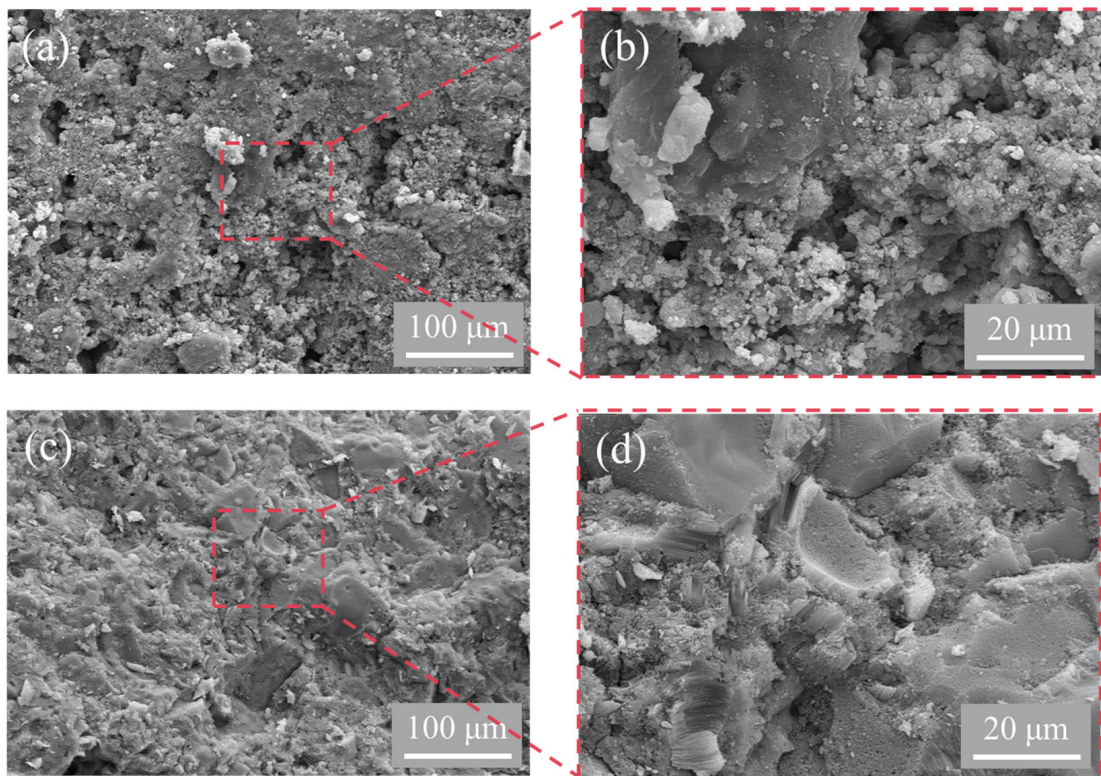


Figure 12. The surface microstructure of the RCA: (a,b) no modification; (c,d) SCA modification.

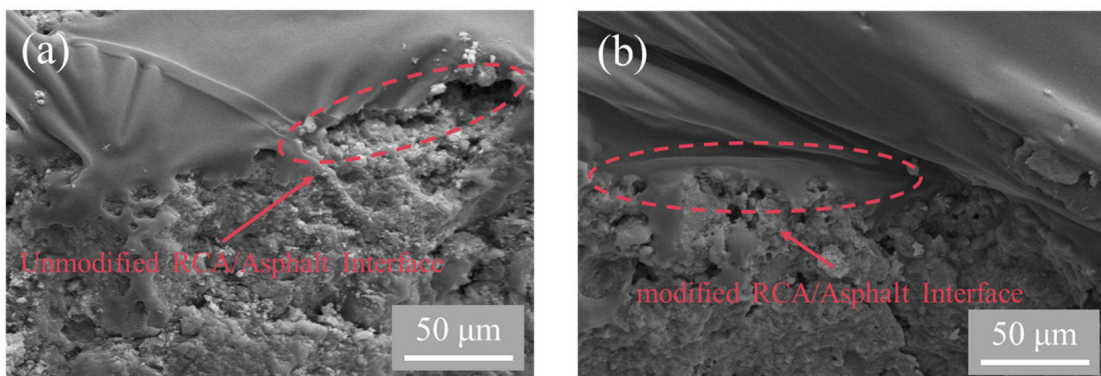


Figure 13. The interface microstructure of the RCA/asphalt: (a) no modification; (b) SCA modification.

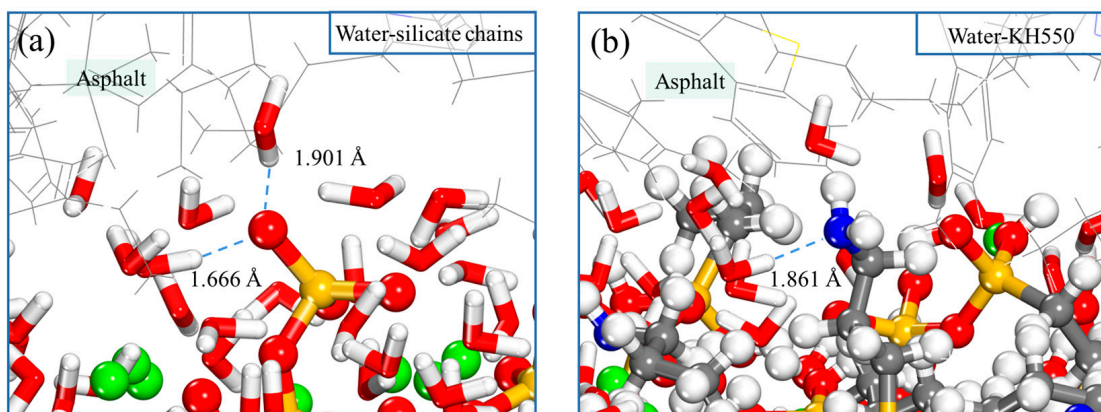


Figure 14. Type of hydrogen bond: (a) water-silicate chains; (b) water-SCA (KH550).

The number of hydrogen bonds formed between C-S-H and interfacial water is shown in Figure 15. The results indicate that there are fewer hydrogen bonds between C-S-H and interfacial water after SCA modification. Specifically, unmodified C-S-H forms 213 hydrogen bonds with interfacial water. The more hydrogen bonds form between C-S-H and interfacial water, the stronger the hydrophilicity of the C-S-H surface. Due to the hydrophobic nature of asphalt, stronger hydrophilicity of the C-S-H surface leads to weaker adhesion between asphalt and the C-S-H. After SCA modification, the number of hydrogen bonds at the C-S-H interface decreases by 19.7%, indicating a decrease in the hydrophilicity of the C-S-H surface after SCA modification, thereby enhancing the interaction at the asphalt/C-S-H interface. This is mainly because the C-S-H surface is composed of silicate chains and calcium ions, which have strong hydrophilicity. After SCA modification, the distance between interfacial water and the C-S-H surface is increased, thereby reducing the formation of hydrogen bonds and decreasing the hydrophilicity of the C-S-H surface. Compared to the previous SCA-modified SiO₂ interface, the SCA modification can be very effective in reducing the hydrophilicity of both SiO₂ and C-S-H surfaces, thus improving the effect of water molecules on the aggregate/interface [60]. The results show that SCA modification has a positive effect on enhancing the water damage resistance of the aggregate/asphalt interface.

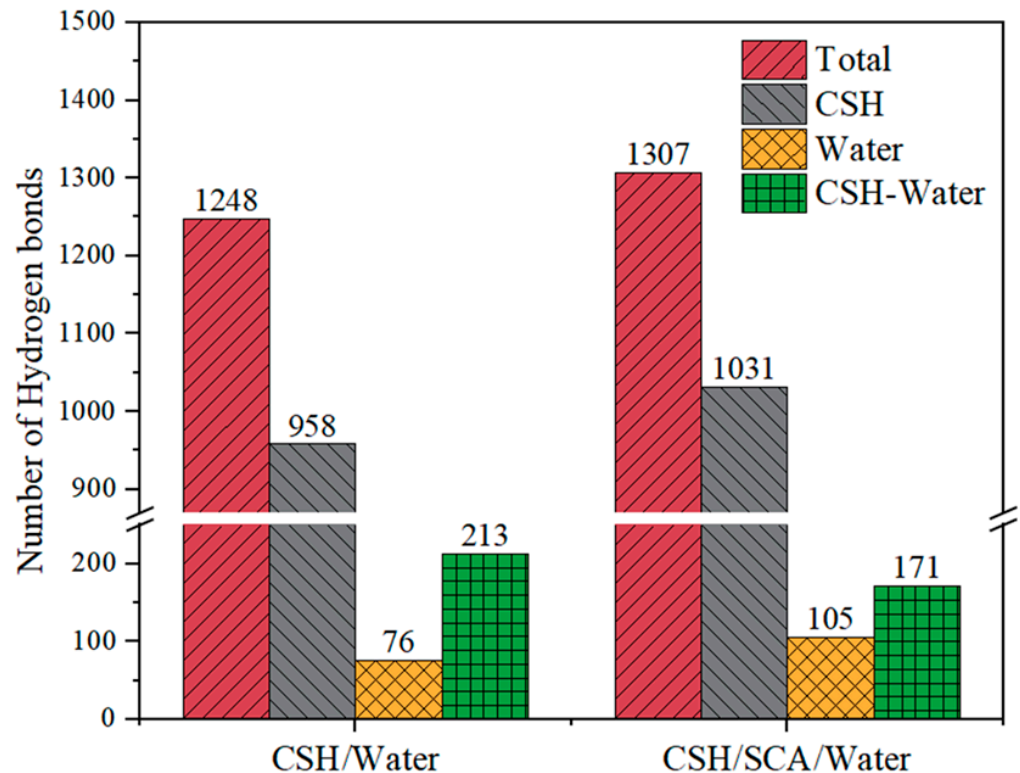


Figure 15. The number of hydrogen bonds for C-S-H/water interface.

4.5. Interaction Energy Analysis

The interaction energy between C-S-H and asphalt is shown in Figure 16. The results indicate that SCA modification can increase the interaction energy of the interface under both dry and wet conditions. Under dry conditions, the interface interaction energy of the SCA modification increased by 32.1%. This increase is attributed to the ability of SCA modification to alleviate the harmful effects of Ca ions and water molecules on the C-S-H surface, thereby improving the interaction energy of the interface. Under wet conditions, the interaction energy of the interface decreased by 47.15%. This is primarily due to the fact that the interaction energy of the interface is mainly governed by van der Waals forces, and the presence of water at the interface increases the distance between the asphalt and

C-S-H interface, resulting in a 48.2% reduction in van der Waals forces. Consequently, the interaction energy of the interface decreases. In comparison, the SCA modification under wet conditions showed a 63.9% increase in interaction energy compared to the unmodified interface. This indicates that SCA modification can effectively enhance the water resistance of the interface. This is because SCA modification reduces the hydrophilicity of the C-S-H interface, diminishing the impact of water molecules on the interface performance and consequently increasing the interaction energy at the asphalt and C-S-H interface.

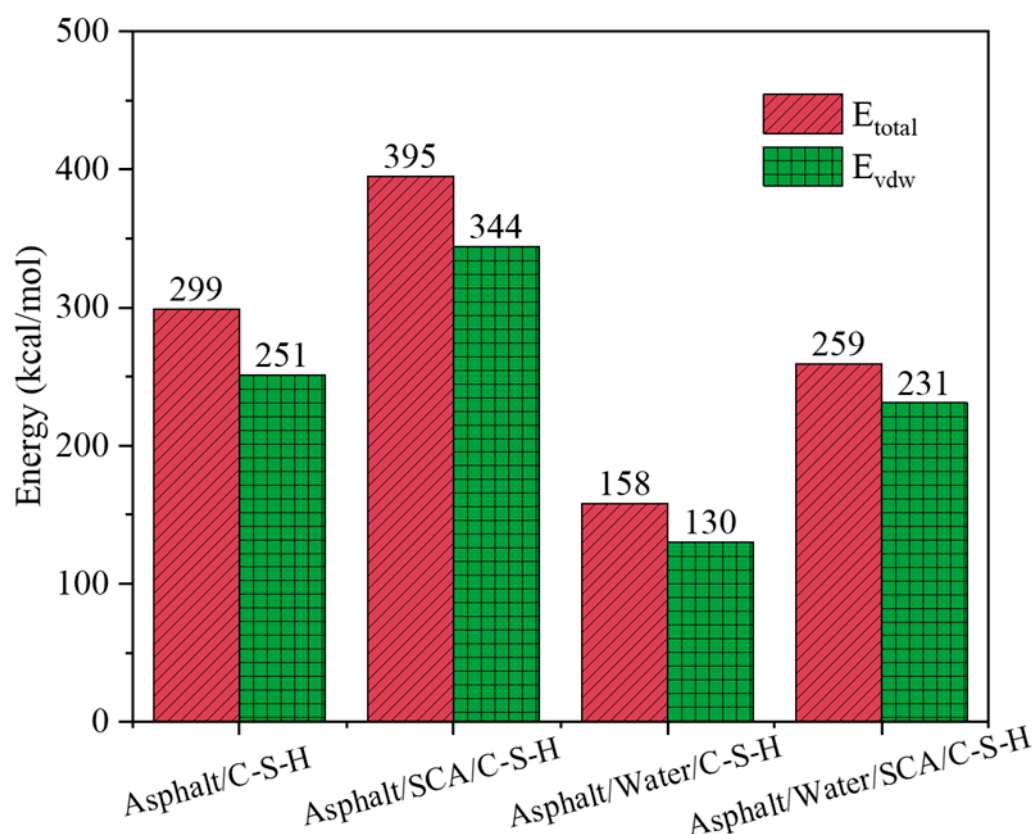


Figure 16. Interaction energy for C-S-H/asphalt interface.

4.6. Interface Transition Zone Analysis

The thickness of the interface transition zone and interface structure for the C-S-H/asphalt interface are shown in Figure 17. It can be seen that SCA modification has an important impact on the transition zone thickness and interface structure. For the unmodified interface, the thickness of the transition zone is 5.04 Å. This may be due to the diffusion of water molecules in C-S-H into the area near the surface of the asphalt, where the water molecules overlap with the asphalt molecules. After SCA modification, the thickness of the transition zone increased from 5.04 Å to 11.2 Å, indicating that SCA modification enhanced the attraction of the C-S-H surface to asphalt. Moreover, two distribution patterns of SCA molecular chains on the C-S-H surface can be observed at the interface structure between C-S-H and asphalt: one is parallel to the C-S-H surface, and the other is inserted into the asphalt layer. The insertion of SCA molecular chains into the asphalt layer is strongly entangled with asphalt molecules, thereby enhancing the weak interface transition zone between C-S-H and asphalt.

The influence of interface water on the asphalt nanostructure is shown in Figure 18. The results indicate that SCA modification reduces the effect of water on the relative concentration of SARA components at the interface. For the unmodified interface, interface water causes a varying degree of decrease in the relative concentration of asphalt SARA components within 0–7 Å. This is why the interaction energy between

asphalt and C-S-H decreases when interface water exists. Within the distance of 7–15 Å, the relative concentration of asphaltene, aromatics, and resins increases, indicating that the addition of water molecules causes the asphalt components at the interface to aggregate towards the center, also demonstrating the hydrophobicity of asphalt. After SCA modification, the relative concentration of resins and aromatics at the interface within 0–5 Å remains basically unchanged, while the concentration of saturates slightly increases. It is worth noting that the relative concentration of asphaltene increases at 4–8 Å and forms a peak. This indicates that after SCA modification, the interface structure of SARA components can remain relatively stable even under the action of water, thereby increasing the resistance to water damage between C-S-H and asphalt.

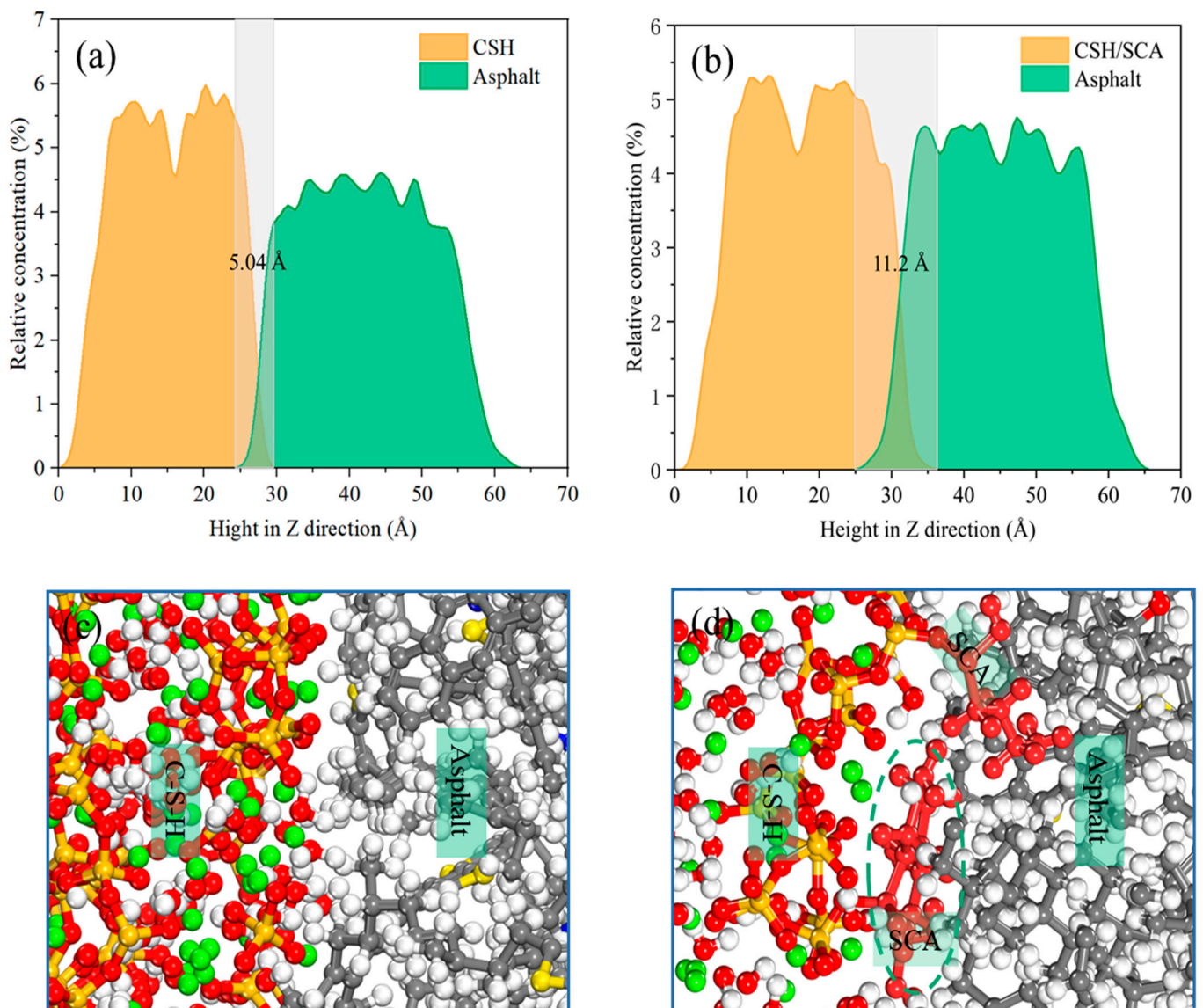


Figure 17. Interface transition zone thickness and interface structure for C-S-H/asphalt interfaces: (a) C-S-H/asphalt interface zone thickness; (b) C-S-H/SCA/asphalt interface transition zone thickness; (c) C-S-H/asphalt interface structure; (d) C-S-H/SCA/asphalt interface structure.

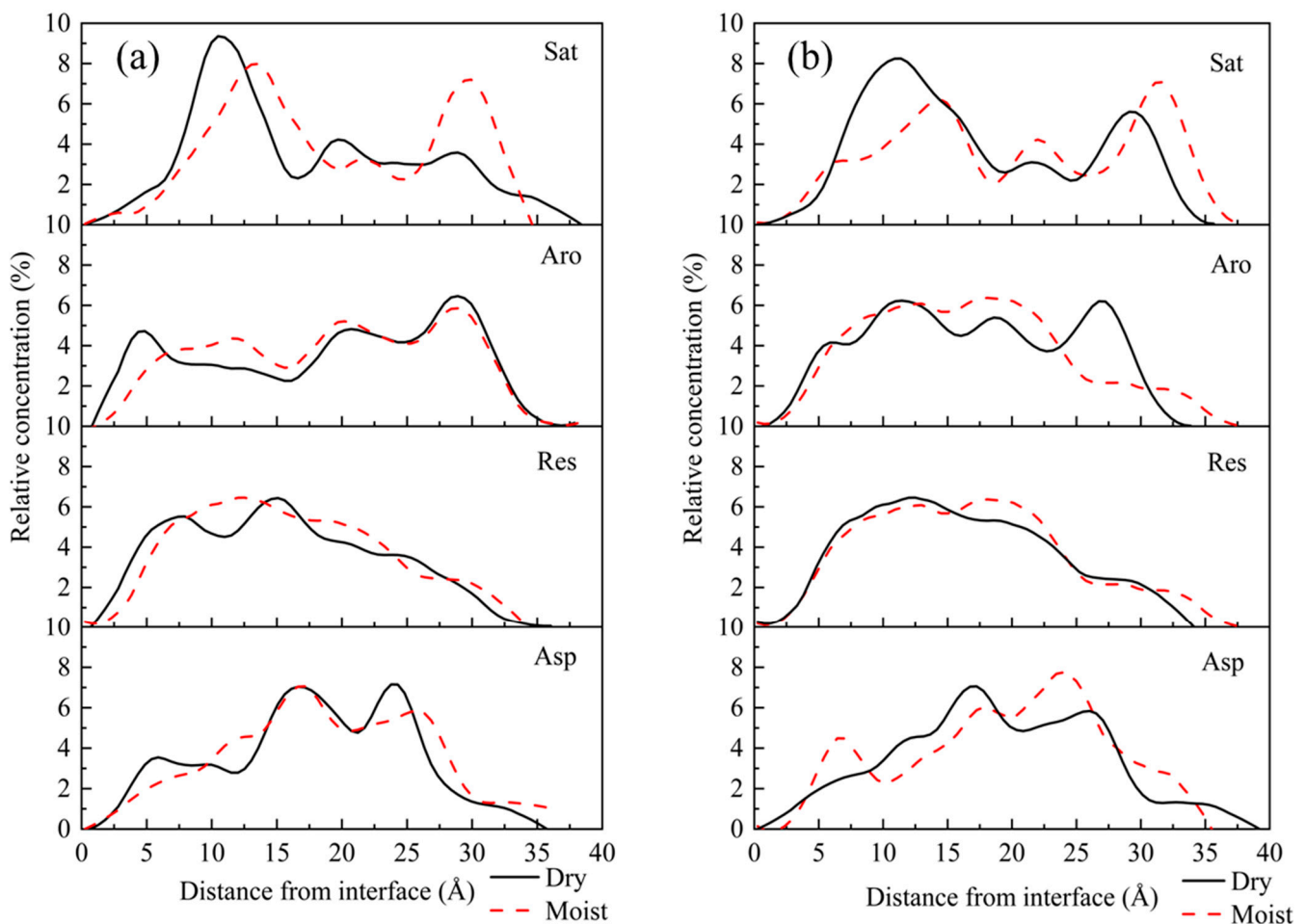


Figure 18. The concentration profiles of SARA components: (a) C-S-H/water/asphalt model; (b) C-S-H/SCA/water/asphalt model.

5. Conclusions

Based on macroscopic experiments, microscopic structure observation, and molecular dynamics simulation, this study examined the enhancement effect of SCA modification on the interface performance of RCA and asphalt before and after modification and investigates its underlying mechanism for enhancement. The following findings were made.

The results of the boiling water experiment and direct tensile experiment indicate that SCA modification significantly improves the interface behavior between RCA and asphalt. The bond between SCA-modified RCA and asphalt is enhanced by two grades, and the tensile strength goes up by 72.2% in dry conditions and 119.7% in wet conditions.

The observation results of SEM show that SCA modification effectively improves the interface structure defects between RCA and asphalt. Before SCA modification, there are numerous pores on the surface of RCA, resulting in structural defects between the RCA and asphalt interface. After SCA modification, a dense film is formed on the surface of the RCA, effectively filling the pores of the RCA surface mortar and creating a more compact bond at the RCA/asphalt interface.

The results of the molecular dynamics simulations indicate that SCA modification reduces the number of hydrogen bonds formed between C-S-H and water molecules, thereby decreasing the hydrophilicity of the C-S-H surface. SCA modification also improves the interaction energy and water resistance of C-S-H with asphalt. Additionally, SCA molecules can penetrate the asphalt layer to create a dense interfacial transition zone between C-S-H and asphalt. This makes the two substances work better together and reduces the effect of water on the nanoscale structure of the asphalt interface.

The study findings help us understand the mechanisms of interfacial interactions between asphalt and modified aggregate surfaces and develop more effective interface modifications. In addition, it lays the foundation for the application of RCA/asphalt mixtures on road surfaces and for improving the road performance of asphalt mixtures. Future research can consider the influence of SCA modification on the interactions between different interfaces, such as SiO_2 /asphalt, CaCO_3 /asphalt, etc. The interaction mechanism of SCA modification on RCA/asphalt interface is explained from a more comprehensive perspective.

Author Contributions: Conceptualization, K.H.; methodology, J.Z.; software, J.Z.; validation, J.Z.; formal analysis, J.Z.; investigation, J.Z.; resources, J.Z.; data curation, J.Z.; writing—original draft preparation, J.Z. and X.D.; writing—review and editing, J.Z. and Y.C.; visualization, J.Z.; supervision, K.H. and Q.Y.; project administration, K.H. and J.G.; funding acquisition, K.H. All authors have read and agreed to the published version of the manuscript.

Funding: This work was financially supported by the Fundamental Research Fund of Natural Science Foundation of China (No. 52208434), the Central Public Welfare Research Institute (No. 2020-9049), Natural Science Foundation of Henan Province (No. 222300420142), Postdoctoral Fund of Henan Province; Science and Technology Project of Henan Province (No. 192102310229), China Postdoctoral Science Foundation (No. 2022M711079), and Young backbone teachers plan of Henan University of Technology (No. 21420156).

Institutional Review Board Statement: Not applicable.

Informed Consent Statement: Not applicable.

Data Availability Statement: All data from this study are presented in the paper.

Conflicts of Interest: The authors declare no conflict of interest.

References

- Xiao, J.; Shen, J.; Gao, Q.; Wu, Y. Reuse of construction spoil in China: Current status and future opportunities. *J. Clean. Prod.* **2020**, *290*, 125742. [[CrossRef](#)]
- Piccinali, A.; Diotti, A.; Plizzari, G.; Plizzari, G. Impact of recycled aggregate on the mechanical and environmental properties of concrete: A review. *Materials* **2022**, *15*, 1818. [[CrossRef](#)]
- Ulucan, M.; Alyamac, K.E. A holistic assessment of the use of emerging recycled concrete aggregates after a destructive earthquake: Mechanical, economic and environmental. *Waste. Manag.* **2022**, *146*, 53–65. [[CrossRef](#)]
- Chen, X.; Yang, Y.; Zhang, C.; Hu, R.; Zhang, H.Y.; Li, B.X.; Zhao, Q.L. Valorization of construction waste materials for pavements of sponge cities: A review. *Constr. Build. Mater.* **2022**, *356*, 129247. [[CrossRef](#)]
- Pal, S.; Mandal, I. Impacts of stone mining and crushing on environmental health in Dwarka river basin. *Geocarto Int.* **2021**, *36*, 392–420. [[CrossRef](#)]
- Hua, C.X.; Liu, C.Y.; Chen, J.G.; Yang, C.X.; Chen, L.Y. Promoting construction and demolition waste recycling by using incentive policies in China. *Environ. Sci. Pollut. R.* **2022**, *29*, 53844–53859. [[CrossRef](#)]
- Molla, A.S.; Tang, P.T.; Sher, W.; Bekele, D.N. Chemicals of concern in construction and demolition waste fine residues: A systematic literature review. *J. Environ. Manag.* **2021**, *299*, 113654. [[CrossRef](#)]
- Liu, H.B.; Liu, H.B.; Quan, H.Z.; Xu, X.L.; Wang, Q.Y.; Ni, S.Y. Assessment on the Properties of Biomass-Aggregate Geopolymer Concrete. *Appl. Sci.* **2022**, *12*, 3561. [[CrossRef](#)]
- Mistri, A.; Dharmi, N.; Bhattacharyya, S.K.; Barai, S.V.; Mukherjee, A.; Biswas, W.K. Environmental implications of the use of bio-cement treated recycled aggregate in concrete. *Resour. Conserv. Recycl.* **2021**, *167*, 105436. [[CrossRef](#)]
- Ni, S.Y.; Liu, H.B.; Li, Q.Y.; Quan, H.Z.; Gheibi, M.; Fathollahi-Fard, A.M.; Tian, G.D. Assessment of the engineering properties, carbon dioxide emission and economic of biomass recycled aggregate concrete: A novel approach for building green concretes. *J. Clean. Prod.* **2022**, *365*, 132780. [[CrossRef](#)]
- Wang, R.J.; Yu, N.N.; Li, Y. Methods for improving the microstructure of recycled concrete aggregate: A review. *Constr. Build. Mater.* **2020**, *242*, 118164. [[CrossRef](#)]
- Martinez-Lage, I.; Vazquez-Burgo, P.; Vazquez-Burgo, P. Sustainability evaluation of concretes with mixed recycled aggregate based on holistic approach: Technical, economic and environmental analysis. *Waste. Manag.* **2020**, *101*, 9–19. [[CrossRef](#)] [[PubMed](#)]
- Colangelo, F.; Petrillo, A.; Farina, I. Comparative environmental evaluation of recycled aggregates from construction and demolition wastes in Italy. *Sci. Total Environ.* **2021**, *798*, 149250. [[CrossRef](#)] [[PubMed](#)]
- Mostert, C.; Sameer, H.; Glanz, D.; Bringezu, S. Climate and resource footprint assessment and visualization of recycled concrete for circular economy. *Resour. Conserv. Recycl.* **2021**, *174*, 105767. [[CrossRef](#)]

15. Gedik, A. A review on the evaluation of the potential utilization of construction and demolition waste in hot mix asphalt pavements. *Resour. Conserv. Recycl.* **2020**, *161*, 104956. [[CrossRef](#)]
16. Liu, C.; Liu, H.W.; Xiao, J.Z.; Bai, G.L. Effect of old mortar pore structure on relative humidity response of recycled aggregate concrete. *Constr. Build. Mater.* **2020**, *247*, 118600. [[CrossRef](#)]
17. Jang, H.; Kim, J.; Kim, J. Effect of aggregate size on recycled aggregate concrete under equivalent mortar volume mix design. *Appl. Sci.* **2021**, *11*, 11274. [[CrossRef](#)]
18. Huang, Q.B.; Qian, Z.D.; Hu, J.; Zheng, D.; Chen, L.L.; Zhang, M.; Yu, J.Z. Investigation on the properties of aggregate-mastic interfacial transition zones (ITZs) in asphalt mixture containing recycled concrete aggregate. *Constr. Build. Mater.* **2021**, *269*, 121257. [[CrossRef](#)]
19. Ji, J.; Li, P.F.; Chen, M.; Zhang, R.; Zhou, W.J.; You, Z.P. Review on the fatigue properties of recycled asphalt concrete containing construction and demolition wastes. *J. Clean. Prod.* **2021**, *327*, 129478. [[CrossRef](#)]
20. Liu, S.J.; Cui, S.P.; Guo, H.X.; Wang, Y.L.; Zheng, Y. Adsorption of lead ion from wastewater using non-crystal hydrated calcium silicate gel. *Materials* **2021**, *14*, 842. [[CrossRef](#)]
21. Prasad, D.; Singh, B.; Suman, S.K. Utilization of recycled concrete aggregate in bituminous mixtures: A comprehensive review. *Constr. Build. Mater.* **2022**, *326*, 126859. [[CrossRef](#)]
22. Foti, D.; Cavallo, D. Mechanical behavior of concretes made with non-conventional organic origin calcareous aggregates. *Constr. Build. Mater.* **2018**, *179*, 100–106. [[CrossRef](#)]
23. Spairani, Y.; Cisternino, A.; Foti, D.; Lerna, M.; Ivorra, S. Study of the behavior of structural materials treated with bioconsolidant. *Materials* **2021**, *14*, 5369. [[CrossRef](#)] [[PubMed](#)]
24. Lerna, M.; Foti, D.; Petrella, A.; Sabbà, M.F.; Mansour, S. Effect of the chemical and mechanical recycling of PET on the thermal and mechanical response of mortars and premixed screeds. *Materials* **2023**, *16*, 3155. [[CrossRef](#)] [[PubMed](#)]
25. Lerna, M.; Caballero-Jorna, M.; Roig-Flores, M.; Foti, D.; Serna, P. Influence of recycled materials on the mechanical properties of macro synthetic fiber-reinforced concrete. In Proceedings of the FIB International Congress, Oslo, Norway, 12–16 June 2022.
26. Gunka, V.; Demchuk, Y.; Sidun, I.; Miroshnichenko, D.; Nyakuma, B.B.; Pyshyev, S. Application of phenol-cresol-formaldehyde resin as an adhesion promoter for bitumen and asphalt concrete. *Road Mater. Pavement Des.* **2021**, *22*, 2906–2918. [[CrossRef](#)]
27. Wang, X.; Zhang, C.S.; Wu, Q.S.; Zhu, H.J.; Liu, Y. Thermal properties of metakaolin-based geopolymer modified by the silane coupling agent. *Mater. Chem. Phys.* **2021**, *267*, 124655. [[CrossRef](#)]
28. Liu, J.M.; Ju, B.Y.; Yin, Q.; Xie, W.; Xiao, H.Y.; Dong, S.L. Properties of Concrete Prepared with silane coupling agent impregnated coral aggregate and coral concrete. *Materials* **2021**, *14*, 6454. [[CrossRef](#)]
29. Luo, X.Y.; Wei, Y.H.; Ma, L.L.; Tian, W.; Zhu, C.Y. Effect of corrosive aging environments on the flexural properties of silane-coupling-agent-modified basalt-fiber-reinforced composites. *Materials* **2023**, *16*, 1543. [[CrossRef](#)]
30. Aziz, T.; Ullah, A.; Fan, H.; Jamil, M.I.; Khan, F.U.; Ullah, R.; Iqbal, M.; Ali, A.; Ullah, B. Recent Progress in Silane Coupling Agent with Its Emerging Applications. *J. Polym. Environ.* **2021**, *29*, 3427–3443. [[CrossRef](#)]
31. Feng, Y.; Wang, W.J.; Wang, S.Q.; Niu, Z.J.; Li, L.Y. Multi-scale analysis of mechanical properties of KH-560 coupling agent modified PVA fiber-rubber concrete. *Compos. Interface* **2023**, *30*, 983–1010. [[CrossRef](#)]
32. Li, Y.L.; Li, Y.Z.; Li, Y.; Liu, Z.Z.; Wen, L.F.; Zhang, Y.Z.; Zhou, H. Effect of silane coupling agent on improving adhesive property between acidic aggregate and hydraulic asphalt. *J. Mater. Civil Eng.* **2021**, *33*, 04021172. [[CrossRef](#)]
33. Ye, Y.L.; Hao, Y.; Zhuang, C.Y.; Shu, S.Q.; Lv, F.L. Evaluation on improvement effect of different anti-stripping agents on pavement performance of granite-asphalt mixture. *Materials* **2022**, *15*, 915. [[CrossRef](#)] [[PubMed](#)]
34. Ran, W.P.; Zhu, H.L.; Shen, X.Z.; Zhang, Y. Rheological properties of asphalt mortar with silane coupling agent modified oil sludge pyrolysis residue. *Constr. Build. Mater.* **2022**, *329*, 127057. [[CrossRef](#)]
35. Guo, F.C.; Pei, J.Z.; Zhang, J.P.; Xue, B.; Sun, G.Q. Study on the adhesion property between asphalt binder and aggregate: A state-of-the-art review. *Constr. Build. Mater.* **2020**, *256*, 119474. [[CrossRef](#)]
36. Hou, D.S.; Yang, Q.R.; Jin, Z.Q.; Wang, P.; Wang, M.H.; Wang, X.P.; Zhang, Y. Enhancing interfacial bonding between epoxy and CSH using graphene oxide: An atomistic investigation. *Appl. Surf. Sci.* **2021**, *568*, 150896. [[CrossRef](#)]
37. Yu, C.H.; Hu, K.; Yang, Q.L.; Chen, Y.J. Multi-scale observation of oxidative aging on the enhancement of high-temperature property of SBS-modified asphalt. *Constr. Build. Mater.* **2021**, *313*, 125478. [[CrossRef](#)]
38. Sun, W.; Wang, H. Moisture effect on nanostructure and adhesion energy of asphalt on aggregate surface: A molecular dynamics study. *Appl. Surf. Sci.* **2020**, *510*, 145435. [[CrossRef](#)]
39. Luo, L.; Chu, L.J.; Fwa, T.F. Molecular dynamics analysis of moisture effect on asphalt-aggregate adhesion considering anisotropic mineral surfaces. *Appl. Surf. Sci.* **2020**, *527*, 146830. [[CrossRef](#)]
40. Zhai, M.; Li, J.L.; Wang, R.R.; Yue, J.C.; Wang, X.F. Revealing mechanisms of aging and moisture on thermodynamic properties and failure patterns of asphalt-aggregate interface from the molecular Scale. *J. Mater. Civil Eng.* **2023**, *35*, 04022486. [[CrossRef](#)]
41. *ASTM D1078-11*; Standard Test Method for Distillation Range of Volatile Organic Liquids. ASTM International: West Conshohocken, PA, USA, 2019.
42. *ASTM D4052*; Standard Test Method for Density, Relative Density, and API Gravity of Liquids by Digital Density Meter. ASTM International: West Conshohocken, PA, USA, 2022.
43. *ASTM D542-14*; Standard Test Method for Index of Refraction of Transparent Organic Plastics. ASTM International: West Conshohocken, PA, USA, 2014.

44. ASTM D5-06; Standard Test Method for Penetration of Bituminous Materials. ASTM International: West Conshohocken, PA, USA, 2017.
45. ASTM D36-06; Standard Test Method for Softening Point of Bitumen (Ring-and-Ball Apparatus). ASTM International: West Conshohocken, PA, USA, 2010.
46. ASTM D113-07; Standard Test Method for Ductility of Bituminous Materials. ASTM International: West Conshohocken, PA, USA, 2018.
47. Liu, T.J.; Wei, H.N.; Zhou, A.; Zou, D.J.; Jian, H.S. Multiscale investigation on tensile properties of ultra-high performance concrete with silane coupling agent modified steel fibers. *Cem. Concr. Compos.* **2020**, *111*, 103638. [[CrossRef](#)]
48. ASTM D36-25; Standard Practice for Effect of Water on Bituminous-Coated Aggregate Using Boiling Water. ASTM International: West Conshohocken, PA, USA, 2012.
49. ASTM D4124-09; Standard Test Method for Separation of Asphalt into Four Fractions. ASTM International: West Conshohocken, PA, USA, 2018.
50. Hu, K.; Yu, C.H.; Chen, Y.J.; Li, W.; Wang, D.D.; Zhang, W.G. Multiscale mechanisms of asphalt performance enhancement by crumbed waste tire rubber: Insight from molecular dynamics simulation. *J. Mol. Model.* **2021**, *27*, 170–184. [[CrossRef](#)] [[PubMed](#)]
51. Hu, K.; Yu, C.H.; Yang, Q.L.; Li, Z.W.; Zhang, W.G.; Zhang, T.L.; Feng, Y. Mechanistic study of graphene reinforcement of rheological performance of recycled polyethylene modified asphalt: A new observation from molecular dynamics simulation. *Constr. Build. Mater.* **2022**, *320*, 126263. [[CrossRef](#)]
52. Yu, C.H.; Yang, Q.L. Investigation of the interfacial interaction of carbon nanomaterials with asphalt matrix: Insights from molecular simulations. *Mol. Simul.* **2023**, *49*, 208–222. [[CrossRef](#)]
53. Qin, D.J.; Feng, Y.; Li, L.J. Molecular dynamics study on improvement effect of polyethylene terephthalate on adhesive properties of asphalt and cement-based composite interface. *Mol. Simul.* **2023**, *49*, 1293–1302. [[CrossRef](#)]
54. Jiang, F.X.; Yang, Q.R.; Wang, Y.T.; Wang, P.; Hou, D.S.; Jin, Z.Q. Insights on the adhesive properties and debonding mechanism of CFRP/concrete interface under sulfate environment: From experiments to molecular dynamics. *Constr. Build. Mater.* **2021**, *269*, 121247. [[CrossRef](#)]
55. Feng, Y.; Li, Y.; Zhao, C.; Qin, D.J.; Wang, C.; Wang, P.Y. Nano-CaCO₃ enhances PVA fiber-matrix interfacial properties: An experimental and molecular dynamics study. *Mol. Simul.* **2022**, *48*, 1378–1392. [[CrossRef](#)]
56. Hou, D.S.; Yang, Q.R.; Wang, P.; Jin, Z.Q.; Wang, M.H.; Zhang, Y.; Wang, X.P. Unraveling disadhesion mechanism of epoxy/CSH interface under aggressive conditions. *Cem. Concr. Compos.* **2021**, *146*, 106489. [[CrossRef](#)]
57. Luo, Q.; Li, Y.Y.; Zhang, Z.; Peng, X.J.; Geng, G.Q. Influence of substrate moisture on the interfacial bonding between calcium silicate hydrate and epoxy. *Constr. Build. Mater.* **2022**, *320*, 126252. [[CrossRef](#)]
58. Luo, Q.; Zhang, X.Y.; Li, Y.Y.; Zhang, Z.; Geng, G.Q. Interfacial degradation of calcium silicate hydrate and epoxy under a hygrothermal environment: An experimental and molecular model study. *J. Phys. Chem. C* **2023**, *127*, 1607–1621. [[CrossRef](#)]
59. Cui, W.T.; Huang, W.K.; Hu, B.; Xie, J.W.; Xiao, Z.C.; Cai, X.; Wu, K.H. Investigation of the Effects of Adsorbed Water on Adhesion Energy and Nanostructure of Asphalt and Aggregate Surfaces Based on Molecular Dynamics Simulation. *Polymers* **2020**, *12*, 2339. [[CrossRef](#)]
60. Cui, B.Y.; Wang, H. Molecular interaction of Asphalt-Aggregate interface modified by silane coupling agents at dry and wet conditions. *Appl. Surf. Sci.* **2022**, *275*, 151365. [[CrossRef](#)]

Disclaimer/Publisher’s Note: The statements, opinions and data contained in all publications are solely those of the individual author(s) and contributor(s) and not of MDPI and/or the editor(s). MDPI and/or the editor(s) disclaim responsibility for any injury to people or property resulting from any ideas, methods, instructions or products referred to in the content.